Cross sections of the ^{56}Fe$(n,\alpha)^{53}$Cr and ^{54}Fe$(n,\alpha)^{51}$Cr reactions in the MeV region

Zhimin Wang, Xiao Fan, Luyu Zhang, Huaiyong Bai, Jinxiang Chen, and Guohui Zhang*
State Key Laboratory of Nuclear Physics and Technology, Institute of Heavy Ion Physics, Peking University, Beijing 100871, China

Yu. M. Gledenov and M. V. Sedysheva
Frank Laboratory of Neutron Physics, Joint Institute for Nuclear Research, Dubna 141980, Russia

L. Krupa
Flerov Laboratory of Nuclear Reactions, Joint Institute for Nuclear Research, Dubna 141980, Russia and
Institute of Experimental and Applied Physics, Czech Technical University in Prague, Horska 3a/22, Prague 2, 12800 Czech Republic

G. Khuukhenkhuu
Nuclear Research Centre, National University of Mongolia, Ulaanbaatar, Mongolia
(Received 7 May 2015; revised manuscript received 9 September 2015; published 7 October 2015)

Cross sections of the ^{56}Fe(n,α) ^{53}Cr and ^{54}Fe(n,α) ^{51}Cr reactions were measured at $E_n = 5.5$ and 6.5 MeV and $E_n = 4.0$, 4.5, 5.5, and 6.5 MeV, respectively, using a double-section gridded ionization chamber as the α-particle detector. Natural iron and enriched ^{56}Fe and ^{54}Fe foil samples were prepared. A deuterium gas target was used to produce monoenergetic neutrons through the ^{2}H(d,n) ^{3}He reaction. Two rounds of experiments were performed at the 4.5-MV Van de Graaff Accelerator of Peking University. The foreground and background were measured in separate runs. The neutron flux was monitored by a BF_3 long counter, and the cross sections of the ^{238}U(n,f) reaction were used as the standard. Present results are compared with those of the TALYS-1.6 code calculations, existing measurements, and evaluations.

DOI: 10.1103/PhysRevC.92.044601 PACS number(s): 28.20.−v, 25.40.−h, 24.10.−i

I. INTRODUCTION

Iron is one of the most important structural materials in nuclear science and engineering. For example, it is considered as one of the highest priority elements in the International Thermonuclear Experimental Reactor and International Fusion Material Irradiation Facility projects [1]. Recently, the CIELO Collaboration international cooperation also put the ^{56}Fe isotope on the first priority list to clarify discrepancies among different nuclear data libraries of evaluations and measurements [2]. The cross-sectional data of charged particle emission reactions induced by neutrons are needed for evaluations of nuclear heating and radiation damage. Due to the (n,α) reaction, in particular, helium gas accumulated in the material causes serious embrittlement problems in reactors and other high-energy installations. So accurate cross-section data for the (n,α) reactions of iron isotopes are in great demand.

Natural iron is composed of four isotopes, i.e., ^{56}Fe (91.754%), ^{54}Fe (5.845%), ^{57}Fe (2.119%), and ^{58}Fe (0.282%) according to the decrease in their abundances [3]. The Q values for ^{56}Fe, ^{54}Fe, ^{57}Fe, and ^{58}Fe(n,α) reactions are 0.326, 0.844, 2.399, and −1.399 MeV, respectively [4]. For the ^{56}Fe(n,α) ^{53}Cr reaction, only two measurements exist in the neutron energy range of 8–15 MeV [5,6], among which only one datum from Ref. [5] at $E_n = 8$MeV is included in the EXFOR library [7]. The measurement data are so scanty mainly because the residual nucleus ^{53}Cr is stable, therefore the commonly used activation technique cannot be used [8]. The two existing measurements were performed using the telescope spectrometer consisting of ΔE-E detectors. For the ^{54}Fe(n,α) ^{51}Cr reaction, on the other hand, the activation method is available, and there have been many experimental results since 1961. However, only four measurements exist at neutron energies below 8 MeV, and there have been large differences as several times among them. Since the (n,α) reaction channel for both ^{56}Fe and ^{54}Fe will open and increase rapidly in the MeV region, accurate cross-sectional data in this energy region are important. Although most of the evaluated nuclear data libraries contain these two reactions, there are large discrepancies among them, both in trend and in magnitude [9]. So, new and accurate measurements are needed to clarify these discrepancies.

We have measured the cross sections of the ^{57}Fe(n,α) ^{54}Cr reaction at $E_n = 5.0$, 5.5, 6.0, and 6.5 MeV in our previous publication [10]. In the present paper, we extended our measurement from the ^{57}Fe(n,α) ^{54}Cr reaction with a higher Q value to ^{56}Fe(n,α) ^{53}Cr and ^{54}Fe(n,α) ^{51}Cr reactions with lower Q values. Two rounds of experiments were performed to measure the cross sections of the ^{56}Fe(n,α) ^{53}Cr reaction at $E_n = 5.5$ and 6.5 MeV and the ^{54}Fe(n,α) ^{51}Cr reaction at $E_n = 4.0$, 4.5, 5.5, and 6.5 MeV.

II. DETAILS OF THE EXPERIMENTS

The experiments were performed for two rounds at the 4.5-MV Van de Graaff accelerator of Peking University, China. In the first round, the ^{56}Fe(n,α) ^{53}Cr reaction was measured at $E_n = 6.5$ MeV using the natural iron samples, and the ^{54}Fe(n,α) ^{51}Cr reaction was measured at

*Corresponding author: guohuizhang@pku.edu.cn

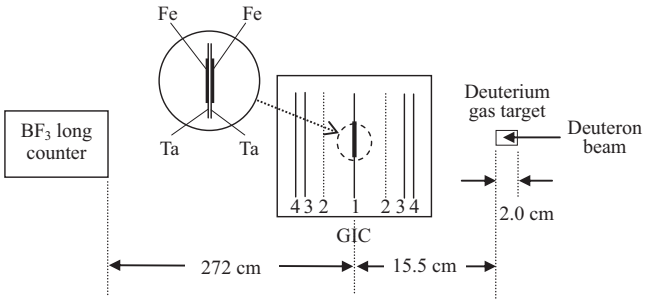

FIG. 1. Schematic of the experimental setup.

FIG. 2. (Color online) Photograph of two enriched ^{56}Fe foil samples.

$E_n = 5.5$ and 6.5 MeV using the enriched ^{54}Fe samples. At higher energy points, the cross sections are relatively bigger, and the accelerator beam durations are shorter. Then, in the second round the ^{56}Fe(n,α) ^{53}Cr reaction was measured at $E_n = 5.5$ and 6.5 MeV using enriched ^{56}Fe samples, and the ^{54}Fe(n,α) ^{51}Cr reaction was measured at $E_n =$ 4.0, 4.5, and 5.5 MeV using the same enriched ^{54}Fe samples as the first round. Measurements in the two rounds were repeated at 6.5 MeV for the ^{56}Fe(n,α) ^{53}Cr reaction and at 5.5 MeV for the ^{54}Fe(n,α) ^{51}Cr reaction to check the reliability of our experiments. Figure 1 is the schematic of the experimental setup which includes three main parts: the neutron source, the charged particle detector (with samples inside), and the neutron flux monitor [10].

Neutrons were produced through the ^{2}H(d,n) ^{3}He reaction by using a deuterium gas target. The monoenergetic neutron energy was changed by adjusting the deuteron beam energy. For neutron energies of 4.0, 4.5, 5.5, and 6.5 MeV, the corresponding neutron energy spreads (1σ) were 0.21, 0.19, 0.14, and 0.10 MeV, respectively [11]. The deuteron beam current was about 3.0 μA during measurements.

The α-particle detector is a double-section gridded ionization chamber (GIC) with a common cathode, and its structure can be found in Ref. [12]. The distance from the cathode to the grid was 61 mm, and that from the grid to the anode was 15 mm. The working gas of the GIC was a mixture gas of krypton with ~3% carbon dioxide. The gas pressures during measurements are listed in Table I. High voltages applied on the cathode and anodes are also included in Table I (the grid electrodes were grounded) which allowed complete collection of electrons from the ionization tracks.

In the present paper, three kinds of foil samples were prepared using natural iron (^{nat}Fe) and highly enriched ^{56}Fe and ^{54}Fe metal materials, respectively. The samples should be thin enough in order to reduce the energy loss and self-absorption of α particles in the sample material. In addition, big area samples are needed because the cross sections to be measured are small and the strengths of the monoenergetic neutron sources in the MeV region are limited. Figure 2 is the photograph of two enriched ^{56}Fe foil samples. The metal foil samples were prepared using the press method with which nearly all material can be utilized without loss. To obtain enough thin and big foil samples, the press process was repeated several times during which the annealing was performed in vacuum for enough times with suitable temperatures. The number of ^{54,56}Fe atoms in the samples was determined by weighing the prepared foils with an accuracy of 1 μg. No oxidization was found in the prepared samples [10]. The shapes of the samples are circular, and data of them are listed in Table II.

A sample changer was set at the common cathode of the ionization chamber with five sample positions, and back-to-back double samples can be placed at each of them [12]. The ^{nat}Fe and enriched ^{54,56}Fe foil samples were attached to the tantalum backings 0.1 mm in thickness. With back-to-back samples, forward (0°−90°) and backward (90°−180°) emitted α particles can be detected simultaneously.

A ^{238}U film sample described in Table II was placed in the GIC at the forward direction of another position of the sample changer to determine the absolute neutron flux by measuring the fission fragments. The standard ^{238}U(n,f) cross-sectional data are taken from the ENDF/B-VII.1 library [9]. Double tantalum sheets and double compound α sources were also placed at other sample positions for (forward and backward) background measurements and energy calibrations, respectively.

The neutron flux monitor is a BF_3 long counter. The axis of the counter was along the normal line of the electrodes

TABLE I. Working gas pressures (atm), cathode and anode high voltages (V) of the GIC in the two rounds of measurements.

E_n (MeV)	First round of measurement		Second round of measurement	
	Natural Fe	^{54}Fe	^{56}Fe	^{54}Fe
4.0				0.52/−1100/550
4.5				0.52/−1100/550
5.5		0.76/−1400/700	0.70/−1500/750	0.70/−1500/750
6.5	0.76/−1400/700	0.76/−1400/700	0.70/−1500/750	

TABLE II. Description of the samples.

Samples	Material	Isotopic abundance (%)	Thickness (μg cm^2)	Diameter (mm)	Backing
^{56}Fe	Natural Fe	91.754	735[a] and 691[b]	44.0[a] and 48.0[b]	Ta sheet
^{56}Fe	Enriched ^{56}Fe	99.94	584[a] and 540[b]	43.5[a] and 44.0[b]	Ta sheet
^{54}Fe	Enriched ^{54}Fe	99.87	555[a] and 557[b]	43.0[a] and 46.0[b]	Ta sheet
^{238}U	$^{238}U_3O_8$	99.999	493.6 (^{238}U only)	45.0	Ta sheet

[a]Forward sample.
[b]Backward sample.

of the ionization chamber as well as the 0° direction of the deuteron beamline. The signals from the BF_3 counter were fed into a scaler (ORTEC 995). A data-acquisition program based on LABVIEW was written to record and display the counts of the BF_3 long counter. The stability of the accelerator neutron source can be displayed from the counts over each period of time (30 s in the present experiments) shown on the screen of the PC as plotted in Fig. 3. The pit in Fig. 3 indicates the variation in the neutron source strength.

Two-dimensional spectra of the cathode-anode coincidence signals for forward and backward directions were recorded separately from which the number of α events from the measured (n,α) reactions can be obtained. The data-acquisition system (DAqS) can be found in Ref. [13]. For each neutron energy point, the experimental process in turn is as follows: (1) compound α-source measurement for energy calibration of the DAqS, (2) foreground measurement for expected α events, (3) background measurement with tantalum sheets, (4) ^{238}U fission fragment measurement for neutron flux calibration with the BF_3 long counter, and (5) α-source measurement again for checking the stability of the DAqS. The beam duration for each reaction at one energy point was 16–28 h. Total beam duration was about 210 h.

Cross sections were determined in the same way as in Ref. [10].

The cross section σ to be measured can be calculated by the following equation:

$$\sigma = \frac{kN_{\rm det}}{\varepsilon}, \tag{1}$$

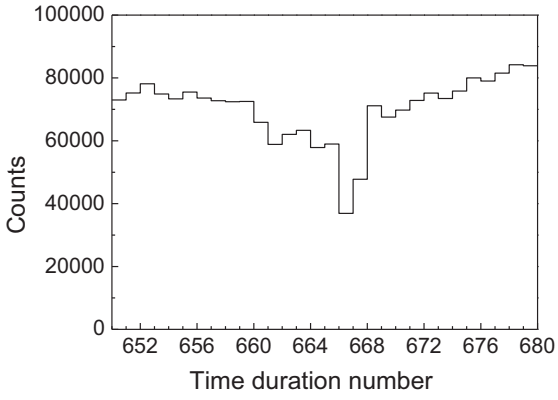

FIG. 3. Counts of the BF_3 long counter over each 30 s.

where $N_{\rm det}$ is the detected counts from the (n,α) reaction above threshold (after background subtraction), ε is the detection efficiency, and k is count-to-cross-sectional factor, which can be written as

$$k = \frac{\sigma_f N_{^{238}\rm U} N_{{\rm BF}_3-f}}{N_f N_{\rm samp} N_{{\rm BF}_3-\alpha}}, \tag{2}$$

where σ_f is the standard ^{238}U(n,f) cross section taken from the ENDF/B-VII.1 library [9], N_f is the number of fission events from the ^{238}U(n,f) reaction, $N_{^{238}\rm U}$ and $N_{\rm samp}$ are the numbers of ^{238}U and ^{54}Fe (or ^{56}Fe) nuclei in the samples, respectively, $N_{{\rm BF}_3-f}$ and $N_{{\rm BF}_3-\alpha}$ are the counts of the neutron flux monitor (BF_3 counter) for ^{238}U fission and for (n,α) event measurements, respectively.

The detection efficiency for α particles and fission fragments,

$$\varepsilon = \frac{N_{\rm det}}{N_{\rm det} + N_{\rm th} + N_{\rm ab}}, \tag{3}$$

where $N_{\rm th}$ is the number of events with amplitudes below threshold (the threshold correction), and $N_{\rm ab}$ is the number of events absorbed in the samples (the self-absorption correction). Values of ε are calculated using the SRIM code [14] to get the stopping power in the samples and the TALYS-1.6 code [15] to predict the angular and energy distributions of the emitted particles.

The cross sections of the ^{54}Fe(n,α) ^{51}Cr and ^{56}Fe(n,α) ^{53}Cr reactions in forward and backward directions can be calculated separately using Eqs. (1)–(3). The complete cross section can be obtained by adding them up together.

III. DATA PROCESSING, RESULTS, AND DISCUSSIONS

The data processing methods are almost the same for both measured (n,α) reactions at all neutron energies. As an example, the following descriptions are given for the data processing of the ^{56}Fe(n,α) ^{53}Cr and ^{54}Fe(n,α) ^{51}Cr reactions at $E_n = 6.5$ MeV for the forward direction in the first round of the experiment.

Figure 4 shows the cathode-anode two-dimensional spectrum of the compound α source, which is used for energy calibration and determination of the 0° and 90° curves. The four groups of α particles, α_1, α_2, α_3, and α_4, with energies of 4.775, 5.155, 5.499, and 5.805 MeV are emitted from the ^{234}U, ^{239}Pu, ^{238}Pu, and ^{244}Cm compound α sources, respectively. The valid α-event area is between the 0° and the 90° curves.

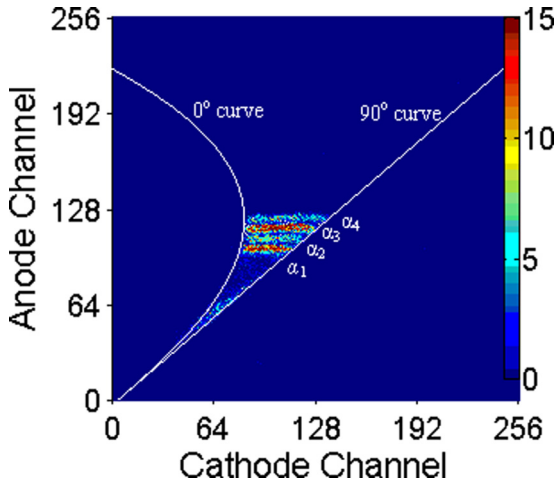

FIG. 4. (Color online) Two-dimensional spectrum of the compound α sources.

Cathode-anode two-dimensional spectra for the foreground and background are plotted from the crude experimental data. Figures 5 and 6 show the results after background subtraction in which the counts between the 0° and the 90° curves represent the α events from the ^{56}Fe(n,α) ^{53}Cr and ^{54}Fe(n,α) ^{51}Cr reactions, respectively. Figures 7 and 8 show the anode spectra after the projection of events between the 0° and the 90° curves in Figs. 5 and 6. As can be seen from the blue curves (pure event), α events corresponding to different energy levels of the residual nuclei cannot be separated, and they become one broad peak due to the close energy levels of the residual nuclei and the energy loss of α particles in the sample. The α counts above the threshold can be obtained from the anode spectrum.

Note that the α counts of the ^{56}Fe(n,α) ^{53}Cr reaction measured in the first round (Fig. 7) need to be corrected because the sample is natural iron, which contains not only ^{56}Fe (91.754%), but also ^{54}Fe (5.845%), ^{57}Fe (2.119%),

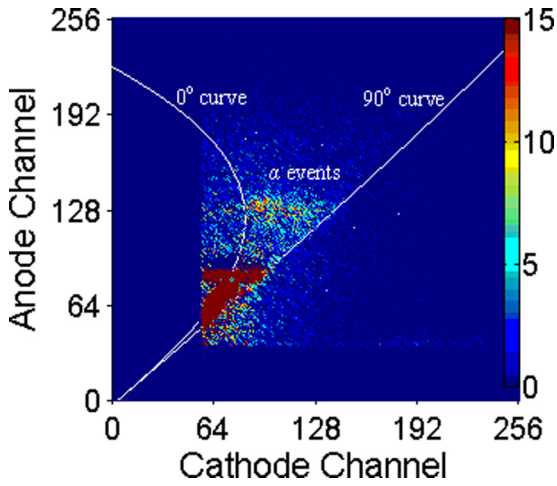

FIG. 5. (Color online) Two-dimensional spectrum of the ^{56}Fe(n,α) ^{53}Cr reaction at $E_n = 6.5$ MeV in the first round of the experiment (forward direction after background subtraction).

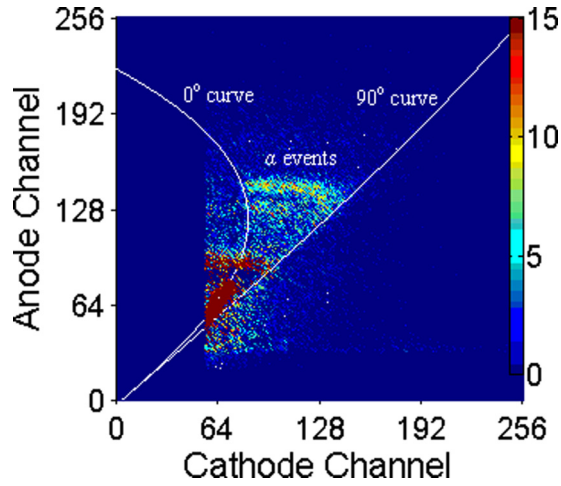

FIG. 6. (Color online) Two-dimensional spectrum of the ^{54}Fe(n,α) ^{51}Cr reaction at $E_n = 6.5$ MeV in the first round of the experiment (forward direction after background subtraction).

and ^{58}Fe (0.282%). The α counts from the ^{54}Fe(n,α) ^{51}Cr, ^{57}Fe $(n,\alpha)^{54}$Cr, and ^{58}Fe $(n,\alpha)^{55}$Cr reactions added up into the spectrum of the ^{56}Fe(n,α) ^{53}Cr reaction. Among which, the α counts from the ^{57}Fe $(n,\alpha)^{54}$Cr and ^{58}Fe $(n,\alpha)^{55}$Cr reactions can be neglected because of the small abundances of ^{57}Fe and ^{58}Fe isotopes and the big differences of the Q values between these two reactions and the ^{56}Fe(n,α) ^{53}Cr reaction [the Q values are 0.326, 2.399, and -1.399 MeV for ^{56}Fe, ^{57}Fe, and ^{58}Fe (n,α) reactions, respectively]. However, the Q value of the ^{54}Fe(n,α) ^{51}Cr reaction is 0.844 MeV, close to that of the ^{56}Fe(n,α) ^{53}Cr reaction of 0.326 MeV, and the abundance of ^{54}Fe is not so small, therefore α counts from the ^{54}Fe(n,α) ^{51}Cr reaction need to be subtracted according to the number of ^{54}Fe nuclei in the natural sample. The anode spectrum of the ^{54}Fe(n,α) ^{51}Cr reaction (Fig. 8) was already obtained in the first round of the experiment using the enriched ^{54}Fe sample, and it was subtracted (according to the number of the ^{54}Fe nuclei and the counts of the BF_3 monitor) from the anode spectrum of the natural iron sample as shown in

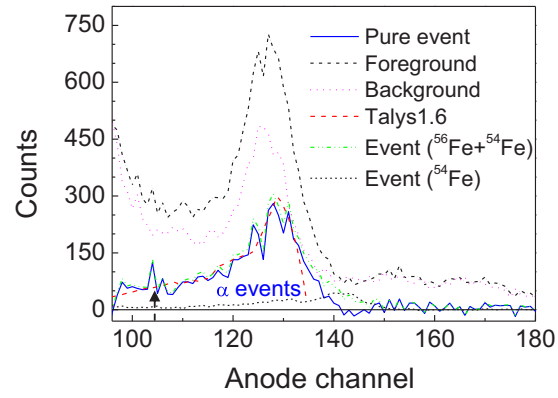

FIG. 7. (Color online) Anode spectrum of the ^{56}Fe(n,α) ^{53}Cr reaction at $E_n = 6.5$ MeV in the first round of the experiment (forward direction).

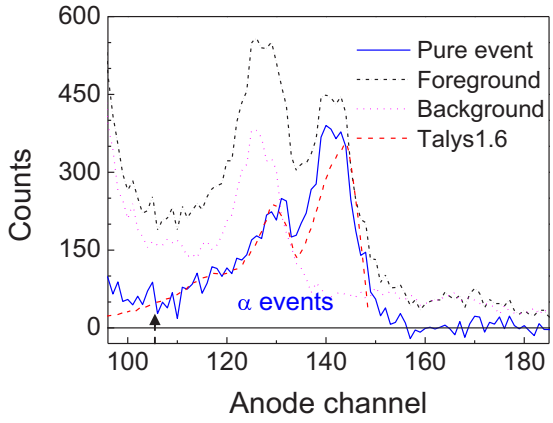

FIG. 8. (Color online) Anode spectrum of the ^{54}Fe(n,α) ^{51}Cr reaction at $E_n = 6.5$ MeV in the first round of the experiment (forward direction).

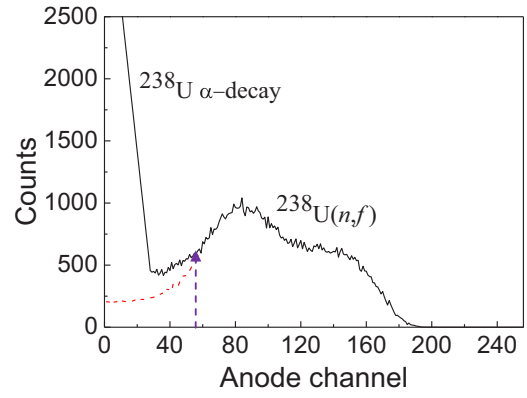

FIG. 9. (Color online) Anode spectrum of the ^{238}U fission fragments at $E_n = 6.5$ MeV in the first round of the experiment.

Fig. 7. About 13% of α counts were subtracted after this correction.

In addition to the α counts above the threshold (arrows shown in Figs. 7 and 8), there are α events below the threshold which cannot be detected. Therefore, the threshold correction and the self-absorption correction are needed as shown in Eq. (3). The simulated anode spectra are shown in Figs. 7 and 8 as the red dashed curves from which the α-particle detection efficiencies were obtained. The simulations were performed using the SRIM [14] and TALYS-1.6 [15] codes to get the stopping power of the α particles in the samples and to predict the angular and energy distributions of the emitted α particles. The calculated α-particle detection efficiency for the ^{56}Fe(n,α) ^{53}Cr reaction is from 65% to 80% and that for the ^{54}Fe(n,α) ^{51}Cr reaction is from 60% to 85% (with an uncertainty of about 5%).

The absolute neutron flux at the sample position was determined by the fission counts from the ^{238}U (n, f) reaction. The anode spectrum of the fission fragments at $E_n = 6.5$ MeV is shown in Fig. 9 from which the fission counts can be obtained after threshold and self-absorption corrections. The correction was made by Monte Carlo simulation using the fission product yield data from the ENDF/B-VII.1 library [9]. The red curve in Fig. 9 shows the simulated spectrum of the fission fragments. The ratio of self-absorption is about 5.8%, and the ratio of the threshold correction is about 15% (with an uncertainty of 25%). The uncertainty of the fission counts is about 3.0%. And using the standard ^{238}U(n, f) cross sections taken from the ENDF/B-VII.1 library [9], the neutron flux can be determined with an uncertainty of 3.4%.

The measured results of the cross sections for the ^{56}Fe(n,α) ^{53}Cr and ^{54}Fe(n,α) ^{51}Cr reactions are listed in Table III. At the repeated energy points [6.5 MeV for the ^{56}Fe(n,α) ^{53}Cr reaction and 5.5 MeV for the ^{54}Fe(n,α) ^{51}Cr reaction], data of the two rounds agree well with each other within measurement uncertainties, which indicates the reliability of the present measurements. Data of the repeated measurements were averaged as the final cross sections. Table III also shows the calculation results using the TALYS-1.6 code with default and adjusted parameters. To fit the present results better, the factor of the potential depth parameter in the optical model v_1 was adjusted from 1 (the default value) to 2 for the ^{56}Fe(n,α) ^{53}Cr reaction and from 1 (the default value) to 1.2 for the ^{54}Fe(n,α) ^{51}Cr reaction. The adjustable range of the parameter v_1 is from 0.1 to 10 [15].

The uncertainties were estimated using the error propagation formula. Sources of uncertainty and their magnitudes are listed in Table IV. The major source of uncertainty is the error of detected α counts (including statistics and background subtraction).

TABLE III. Measured and TALYS-1.6 calculated cross sections for the ^{56}Fe(n,α) ^{53}Cr and ^{54}Fe(n,α) ^{51}Cr reactions.

E_n (MeV)	^{56}Fe		^{54}Fe	
	σ_{exp} (mb)	σ_{TALYS} (mb)	σ_{exp} (mb)	σ_{TALYS} (mb)
4.0			0.76 ± 0.25[b]	0.18,[d] 0.21[e]
4.5			0.36 ± 0.17[b]	0.54,[d] 0.65[e]
5.5	1.05 ± 0.23[b]	0.59,[d] 1.23[e]	3.21 ± 0.38[a], 3.25 ± 0.43[b] 3.23 ± 0.29[c]	3.09,[d] 3.80[e]
6.5	4.57 ± 0.52[a], 5.88 ± 0.79[b] 5.23 ± 0.47[c]	2.31,[d] 4.62[e]	12.86 ± 1.13[a]	9.64,[d]13.37[e]

[a]Results measured in the first round of the experiment.
[b]Results measured in the second round of the experiment.
[c]Averaged over the first and second rounds of cross-sectional data.
[d]Predictions of TALYS-1.6 with default parameters.
[e]Predictions of TALYS-1.6 with adjusted parameters.

TABLE IV. Sources of uncertainty and their magnitudes.

Sources of uncertainty	Magnitude (%)
Counting uncertainty for α particles	12–20[a] and 8–30[b]
Detection efficiency for α particles	5.0
Fission counts of ^{238}U	3.0
Normalization of the BF_3 counts	1.5
Numbers of the ^{56}Fe or ^{54}Fe nucleus	1.0
Numbers of the ^{238}U nucleus	1.3
^{238}U (n, f) cross sections	1.0

[a]For the ^{56}Fe(n,α) ^{53}Cr reaction.
[b]For the ^{54}Fe(n,α) ^{51}Cr reaction.

The final results of the present paper are compared with those of existing measurements, evaluations, and TALYS-1.6 calculations as shown in Figs. 10 and 11. For the ^{56}Fe(n,α) ^{53}Cr reaction as shown in Fig. 10, only two measurements (at four energy points) exist with big uncertainties. As a result, there are large deviations among different evaluation libraries. Our measurements at 5.5 and 6.5 MeV support the data of the JENDL-4.0, JEFF-3.2, FENDLE-2.1, and CENDL-3.1 libraries in the MeV region. Further measurement for the ^{56}Fe(n,α) ^{53}Cr reaction at neutron energies higher than 7 MeV is necessary. For the ^{54}Fe(n,α) ^{51}Cr reaction as shown in Fig. 11, many measurement results exist for neutron energies

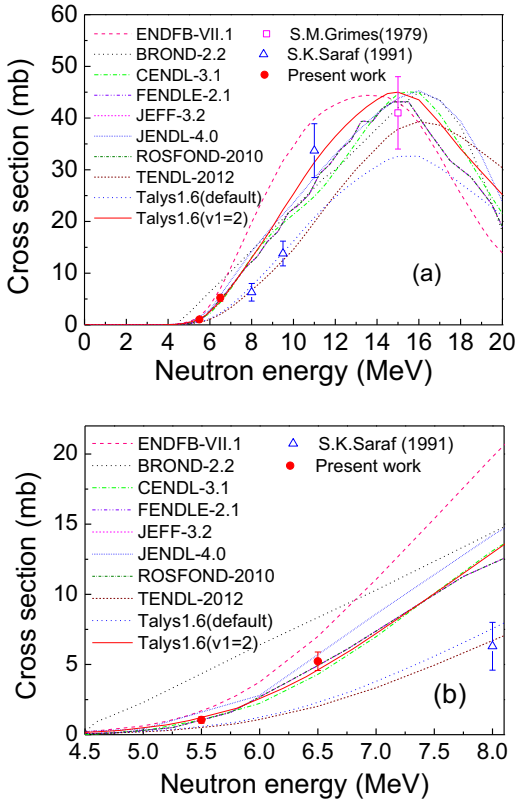

FIG. 10. (Color online) Present cross sections of the ^{56}Fe(n,α) ^{53}Cr reaction compared with existing measurements and evaluations for the neutron energy region (a) from 0 to 20 MeV and (b) from 4.5 to 8.0 MeV.

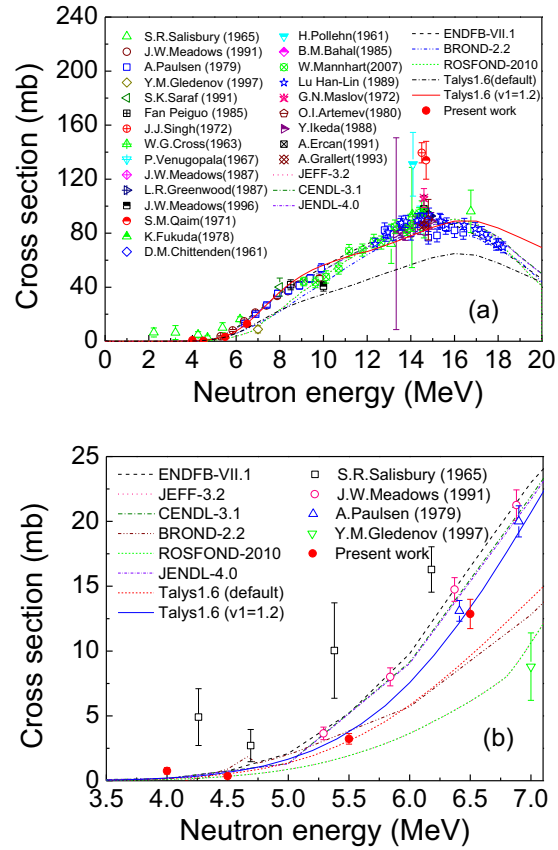

FIG. 11. (Color online) Present cross sections of the ^{54}Fe(n,α) ^{51}Cr reaction compared with existing measurements and evaluations for the neutron energy region (a) from 0 to 20 MeV and (b) from 3.5 to 7.0 MeV.

up to 20 MeV. However, at neutron energies below 7 MeV only four measurements exist, among which large uncertainties exist in Salisbury's measurement data. Our results agree with those of Meadows and Paulsen measured using the activation technique. Our data are smaller in magnitude than those of Salisbury's measurements and bigger than the preliminary datum of Gledenov *et al.*

IV. CONCLUSIONS

In the present paper, cross sections for the ^{56}Fe(n,α) ^{53}Cr reaction at $E_n = 5.5$ and 6.5 MeV and for the ^{54}Fe(n,α) ^{51}Cr reaction at $E_n = 4.0$, 4.5, 5.5, and 6.5 MeV are measured in two rounds of experiments. Agreements of the results between the two rounds indicated the reliability of the present measurements. Our results are generally in agreement with TALYS-1.6 calculations. For the ^{56}Fe(n,α) ^{53}Cr reaction, only two measurements exist with big uncertainties, and there are big disagreements among the evaluated libraries. Our experimental results support most of the evaluated data libraries, such as JENDL-4.0, JEFF-3.2, FENDLE-2.1, and CENDL-3.1. For the ^{54}Fe(n,α) ^{51}Cr reaction, there are four measurements in the neutron energy range below 7 MeV. Present results agree with existing measurements of Meadows and Paulsen using the activation method and are smaller in magnitude than

those of Salisbury and bigger than the preliminary datum of Gledenov *et al.* Our measurement results are useful in the revision of nuclear data libraries as well as in practical applications and for testing of nuclear models. Further measurements of the ^{56}Fe(n,α) ^{53}Cr and ^{54}Fe(n,α) ^{51}Cr reactions at neutron energies higher than 7 MeV are planned.

ACKNOWLEDGMENTS

The authors are indebted to the operation crew of the 4.5-MV Van de Graaff accelerator of Peking University. The present paper was financially supported by the National Natural Science Foundation of China (Grants No. 11175005 and No. 11475007) and the China Nuclear Data Center.

[1] U. Fisher, P. Batistoni, E. Cheng, R. A. Forrest, and T. Nishitani, in *Nuclear Data for Fusion Energy Technologies: Requests, Status and Development Needs*, edited by R. C. Haight, M. B. Chadwick, T. Kawano, and P. Talou, AIP Conf. Proc. No. 769 (AIP, New York, 2005), p. 1478.

[2] M. B. Chadwick, E. Dupont, E. Bauge, A. Blokhin *et al.*, Nuclear Data Sheets **118**, 1 (2014).

[3] NUDAT2, National Nuclear Data Center, Brookhaven National Laboratory, version 2.6 [http://www.nndc.bnl.gov/nudat2].

[4] Q-value calculator, National Nuclear Data Center, Brookhaven National Laboratory [http://www.nndc.bnl.gov/qcalc/].

[5] S. K. Saraf, C. E. Brient, P. M. Egun, S. M. Grimes, V. Mishra, and R. S. Pedroni, Nucl. Sci. Eng. **107**, 365 (1991).

[6] S. M. Grimes, R. C. Haight, K. R. Alvar, H. H. Barschall, and R. R. Borchers, Phys. Rev. C **19**, 2127 (1979).

[7] EXFOR: Experimental Nuclear Reaction Data, database version of January 7, 2015 [https://www-nds.iaea.org/exfor/exfor.htm].

[8] P. M. Prajapati, B. Pandey, C. V. S. Rao, S. Jakhar, T. K. Basu, B. K. Nayak, S. V. Suryanarayana, and A. Saxena, Fusion Sci. Technol. **66**, 426 (2014).

[9] ENDF: Evaluated Nuclear Data File, database version of October 22, 2014 [https://www-nds.iaea.org/exfor/endf.htm].

[10] Y. M. Gledenov, M. V. Sedysheva, V. A. Stolupin, G. Zhang, J. Han, Z. Wang, X. Fan, X. Liu, J. Chen, G. Khuukhenkhuu, and P. J. Szalanski, Phys. Rev. C **89**, 064607 (2014).

[11] G. Zhang, Y. M. Gledenov, G. Khuukhenkhuu, M. V. Sedysheva, P. J. Szalanski, P. E. Koehler, Y. N. Voronov, J. Liu, X. Liu, J. Han, and J. Chen, Phys. Rev. Lett. **107**, 252502 (2011).

[12] X. Zhang, Z. Chen, Y. Chen, J. Yuan, G. Tang, G. Zhang, J. Chen, Y. M. Gledenov, G. Khuukhenkhuu, and M. Sedysheva, Phys. Rev. C **61**, 054607 (2000).

[13] G. Zhang, H. Wu, J. Zhang, J. Liu, J. Chen, Y. M. Gledenov, M. V. Sedysheva, G. Khuukhenkhuu, and P. J. Szalanski, Eur. Phys. J. A **43**, 1 (2010).

[14] J. F. Ziegler, SRIM-2013, http://www.srim.org/#SRIM.

[15] A. Koning, S. Hilaire, and S. Goriely, *User Manual of talys-1.6* (Nuclear Research and Consultancy Group, Petten, The Netherlands, 2013), p. 43.